

Cite this: *CrystEngComm*, 2011, **13**, 4617

www.rsc.org/crystengcomm

PAPER

Aggregation-induced emission enhancement materials with large red shifts and their self-assembled crystal microstructures†

Qing Dai,^a Weimin Liu,^a Lintao Zeng,^a Chun-Sing Lee,^{*b} Jiasheng Wu^a and Pengfei Wang^{*a}

Received 10th January 2011, Accepted 14th April 2011

DOI: 10.1039/c1ce05035d

Two simple intramolecular charge transfer compounds (BzBMN and BzFAN), derived from 2-benzyloxy-4-diethylaminobenzaldehyde, have been synthesized. Unlike typical AIEE molecules, the enhanced emission of these compounds in the solid state is accompanied by large red shifts in emission wavelength. Absorption and photoluminescence (PL) spectra of the compounds in solution, film and the X-ray single crystal structures were investigated to understand the mechanism of enhanced emission in the solid state. The results indicate that the bathochromic shift excimer-like emissions originated from dimers induced by the dipole–dipole interaction and long-range ordered arrangement (*e.g.* *J*-aggregation), and the enhanced emission is attributed to the restriction of intramolecular rotations caused by multiple intermolecular hydrogen bonding interactions. In addition, it was also observed that BzBMN and BzFAN can facilely form single crystal microbelts and microtubes by a simple reprecipitation method.

Introduction

Organic materials with a strong solid-state emission have received great attention for their important applications in the fundamental research field of solid-state photochemistry and in the applied field of optoelectronic devices.¹ However, for most organic fluorophores, the effects of aggregation-caused quenching (ACQ) have limited their large-scale applications.² Many efforts have been made to overcome the ACQ problems, such as the introduction of bulky substituents onto the original chromophores or doping them into matrix materials to reduce the extent of aggregation.³ However, unfortunately, fluorophores with high emission in the solid state are still rare. Recently, a few fluorophores, including silole derivatives,⁴ 1,1,2,2-tetraphenylethene (TPE) derivatives,⁵ and 1-cyano-*trans*-1,2-bis-(4-methylphenyl)ethylene (CN-MBE) derivatives,⁶ have been found to show significant enhancement in their light emission upon aggregation or in the solid state. This unusual phenomenon was named aggregation-induced emission

(AIE) by Tang *et al.*, or aggregation-induced emission enhancement (AIEE) by Park *et al.* It offers another possible solution for the ACQ problem and indeed some AIEE active molecules have been shown to be promising emitters in high efficiency optoelectronic devices.^{4c,5b,7} However, materials with AIEE properties are limited and one common feature of these AIEE molecules is that they contain multiple aromatic rings and/or polycyclic aromatic hydrocarbon skeletons.⁸ Moreover, most of them emit blue or green light, while red AIEE emitters are relatively rare.^{2b,9}

On the other hand, 1D nano/microstructured materials have been considered to be important building blocks for miniaturized optoelectronic functional devices.¹⁰ To the best of our knowledge only a few articles report the synthesis of red emitting single crystal 1D organic microbelts or microtubes by the self-assembly of simple molecules.¹¹ Therefore, it is intriguing to develop 1D nanostructures of highly efficient red emitting AIEE materials with simple (few aromatic rings) molecular structures.

In this paper, we prepared two intramolecular charge-transfer (ICT) compounds (BzFAN and BzBMN) with simple structures based on 2-benzyloxy-4-diethylaminobenzaldehyde with formylacrylonitrile or malononitrile as the electron-acceptor. These molecules show a good AIEE character and a tunable orange or red emission. The absorption and PL spectra of the compounds in solution, nanosuspensions, film, and their crystal structures were investigated to elucidate the mechanism of enhanced emission in the aggregation state. Moreover, 1D single crystal microbelts and microtubes with high emitting intensity were also prepared by simple reprecipitation method from ethanol/water mixtures. The morphologies and the formation mechanisms of microtubes were also studied and discussed.

^aKey Laboratory of Photochemical Conversion and Optoelectronic Materials, Technical Institute of Physics and Chemistry, Chinese Academy of Sciences, Beijing, 100190, People's Republic of China. E-mail: wangpf@mail.ipc.ac.cn; Fax: +86-10-62554670; Tel: +86-10-82543435

^bCenter of Super-Diamond and Advanced Films (COSDAF), Department of Physics and Materials Science, City University of Hong Kong, Hong Kong SAR, China. E-mail: apcslee@cityu.edu.hk

† Electronic supplementary information (ESI) available: UV-vis and emission spectra in solution, crystal data of BzBMN and BzFAN. CCDC reference numbers 806623 and 806624. For ESI and crystallographic data in CIF or other electronic format see DOI: 10.1039/c1ce05035d

Results and discussion

Synthesis and structural characterization

As shown in Scheme 1, both BzBMN and BzFAN can be synthesized *via* two simple steps. Compound **2** was synthesized with 88% yield from 4-(diethylamino)salicyl-aldehyde (**1**). Then **2** was reacted with corresponding active hydrogen compounds through the Knoevenagel reaction and the residues underwent acid dissociation reaction to give the crude products: BzBMN or BzFAN. The final products were purified by recrystallization in ethanol with high yields (BzBMN, 85% and BzFAN, 45%, respectively) and were characterized by nuclear magnetic resonance (NMR) and high resolution mass spectroscopy (HR MS).

Photophysical properties in solutions

Table 1 lists the absorption and PL peaks of BzFAN and BzBMN in different solvents and their corresponding quantum yields. The absorption peaks (λ_{abs}) of BzFAN and BzBMN range from 420 to 445 nm and show a strong dependence on the solvent polarity. The spectrum exhibits vibrational structure in nonpolar hexane, while it is slightly broadened and becomes structureless in a polar solvent, such as ethanol (Fig. S1a and S2a†). Concurrently with the spectral red shift, the fluorescence quantum yield (Φ_f) is also gradually reduced with an increase in solvent polarity. In a highly polar ethanol solution, for example, fluorescence is almost quenched for both monomers ($\Phi_f = 0.00098$ and 0.00095 for BzBMN and BzFAN, respectively). This behavior is the typical characteristic of an ICT compound.¹² The very low fluorescence quantum yields of BzFAN and BzBMN in monodisperse states might be attributed to the fast free rotations of the diethylamino, benzyloxy, and malononitrile moieties, which relaxes the excited states by nonradiative decay process.¹³

Aggregation-induced enhanced emission behaviors

Diluted solutions of BzBMN or BzFAN in ethanol give weak PL with an emission maximum (λ_{em}) of 480 nm or 485 nm (Fig. 1). By contrast, in ethanol/water ($v/v = 5/95$) solutions, BzBMN and BzFAN give bright emissions, peaked at 582 and 603 nm, respectively. As water is a poor solvent for BzBMN and BzFAN, it can be envisioned that the hydrophobic molecules would cluster together to form aggregates in the aqueous mixtures at such a high water contents (95%). This is further evidenced by the observation of level-off tails in the long-wavelength region of the absorption spectra due to the Mie effect of the nanoparticles

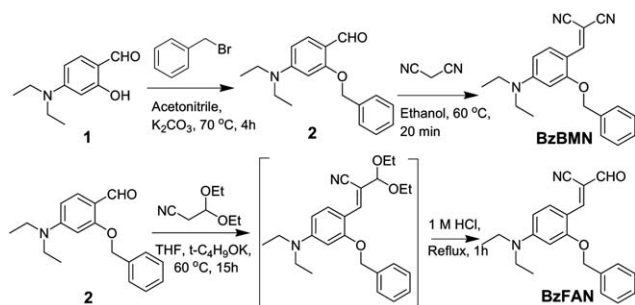
suspension.¹⁴ By using an integrating sphere, we further measured the absolute PL quantum yields of the crystals of BzBMN and BzFAN, which are 0.11 and 0.13, showing 112-fold and 137-fold enhancement, respectively. These show that BzBMN and BzFAN are AIEE active. Fig. 1c–d show fluorescence images of BzBMN and BzFAN in the ethanol solutions, nanoparticle suspensions (95% water) and solid crystal states under UV light. It can be seen that the suspensions have similar emission to the crystals, which indicates that they might have similar microstructures in the aggregates.

The corresponding emission spectra of BzBMN and BzFAN in aqueous ethanol with different ethanol/water ratios are shown in Fig. 2. For solvents with low water contents (<70%), the PL emissions of the compounds are weak and dominated by emission from isolated molecules between 450 and 500 nm. Only when the water fraction is more than 70% do the new emission bands from the aggregates appear and the PL intensities enhance swiftly with the increase of water fraction (insets of Fig. 2).

Mechanisms of emission enhancement

To determine the mechanism of enhanced emission, we measured the PL spectra of BzBMN in an ethanol/methanol solution (4/1 by volume) at low temperature (Fig. 3). The PL intensities are almost the same at temperatures from room temperature to 166 K (the solvents remain in liquid state). When the solution is frozen at 77 K, the PL shows a dramatic increase in intensity and negligible shift in peak wavelength (λ_{em} 476 nm). As there is no intermolecular interaction between BzBMNs in the frozen dilute solution, the PL spectrum represents the characteristics of isolated molecules. The emission enhancement of the BzBMN solution at 77 K is attributed to the restriction of intramolecular rotation in such a rigid solid microenvironment, which shuts down the nonradiative decay. The above results show that the PL spectrum of BzBMN at 77 K is obviously different from that in ethanol/water ($v/v = 5/95$) mixtures. Thus, we can speculate that the AIEE of BzBMN does not originate from isolated molecules but from intermolecular aggregates.

Fig. 4 and 5 show the molecular structures of BzBMN and BzFAN in single crystals determined by X-ray diffraction (Table S1 lists the lattice parameters and structural details†). The dihedral angles for BzBMN and BzFAN between the planes of N2C19N3 (N2C19O2) and the phenyl core are 7.5° and 5.3°, respectively, which show small distortions. This result indicates good planarity along the π -conjugated system in the two molecules, although large twist angles (BzBMN 8.78° and BzFAN 43.50°) between the benzyloxy moiety and central phenyl core exist. Fig. 4b and 5b show how the two neighbor molecules are packed into centrosymmetric anti-parallel (head-to-tail) dimers. Since BzBMN and BzFAN are donor- π -acceptor (D- π -A) dipole molecules, the dipole interaction places the “A” moiety of one molecule above the “D” moiety of another molecule. Besides, π - π stacking interactions may make a contribution to the anti-parallel stacking. Further examination shows that the molecules in the dimer slip over each other along the direction of the long molecular axis (“slipped-parallel” structure). The slipped structure not only avoids the maximum face-to-face stacking that causes the quenched emission, but also favors the dipole-dipole interactions in these ICT compounds. The interplanar



Scheme 1 Synthetic Route of BzBMN and BzFAN.

Table 1 Absorption and emission characteristics of BzBMN and BzFAN in different states

Sample state	BzBMN			BzFAN		
	λ_{abs}^a (nm)	λ_{em}^b (nm)	Φ_f (10^{-3})	λ_{abs}^a (nm)	λ_{em}^b (nm)	Φ_f^c (10^{-3})
In hexane	422	440	1.17 ^c	420	462	1.15 ^c
In toluene	437	468	1.09 ^c	434	464	1.10 ^c
In THF	441	473	1.00 ^c	438	470	1.01 ^c
In ethanol	442	477	0.98 ^c	445	475	0.95 ^c
In methanol	443	483	0.97 ^c	445	480	0.85 ^c
Crystal		567	110 ^d		617	130 ^d

^a Absorption maximum. ^b Emission maximum. ^c Quantum yield ($\pm 10\%$), estimated using 9,10-diphenylanthracene ($\Phi_f = 90\%$ in cyclohexane) as the standard. ^d Absolute quantum yield, determined with an integrating sphere. The spectra were measured in dilute solution with solutes concentration of 20 μM . Excitation wavelength: 410 nm.

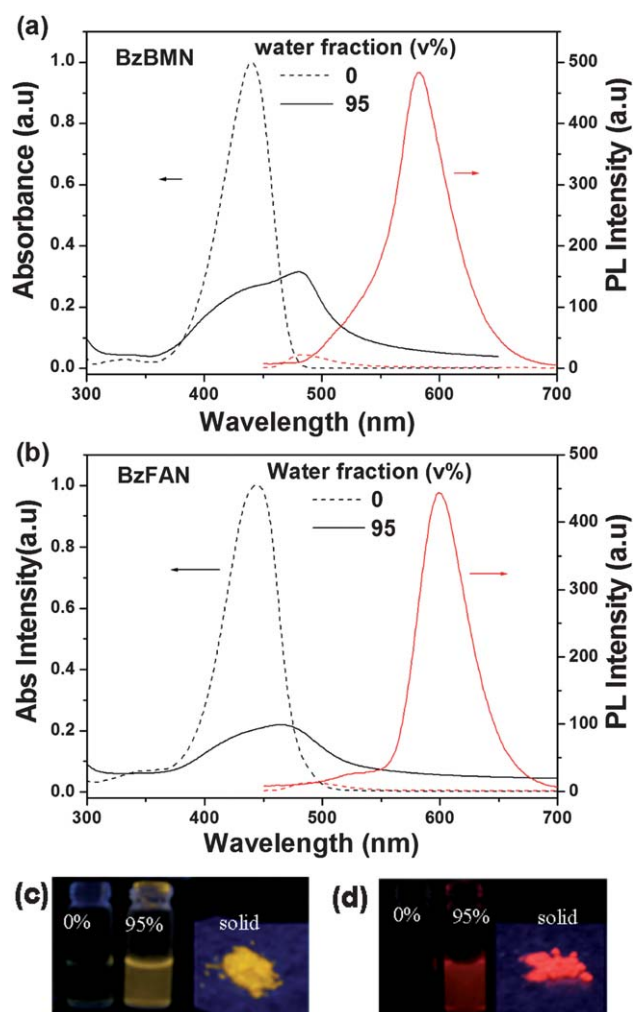


Fig. 1 Absorption (black) and PL (red) spectra of (a) BzBMN and (b) BzFAN in ethanol (dash line) and ethanol/water (5/95, v/v) mixtures with concentration kept at 50 μM . Excitation wavelength: 445 nm. (c), (d) Fluorescent images of BzBMN and BzFAN in ethanol (50 μM), ethanol/water (5/95, v/v) and in the form of solid crystals upon excitation with a 365 nm light source.

spacings of the dimer molecules are 3.573 Å (slip angle, 28.08°) for BzBMN and 3.643 Å (slip angle, 40.90°) for BzFAN, which are larger than the representative π - π stacking interaction

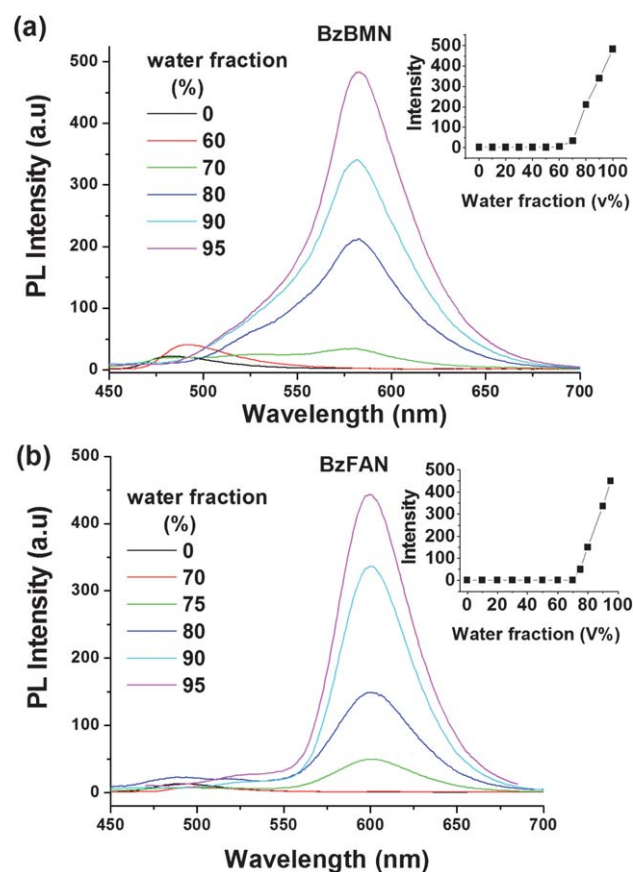


Fig. 2 PL spectra of BzBMN and BzFAN (50 μM) in ethanol/water (v/v) mixtures with different water contents. The insets show the changes in the PL intensity of BzBMN (580 nm) and BzFAN (600 nm) vs. the volume fraction of water in the ethanol/water mixtures.

distances found in other systems.¹⁵ In this circumstance, the π - π stacking interaction is weakened. Thus, we can conclude that dipole-dipole interactions are the main driving forces for dimer formation. The strong dipole interaction is sufficient to cause intermolecular excitonic coupling,¹⁶ which causes the excimer-like emission. Fig. 4e and 5e show that the BzBMN and BzFAN stack into uncontinuous structures with the dimer as the basic building blocks:¹⁷ a larger interplanar spacing and slip angle between different dimer blocks (3.809 Å, 45.11° for BzBMN and

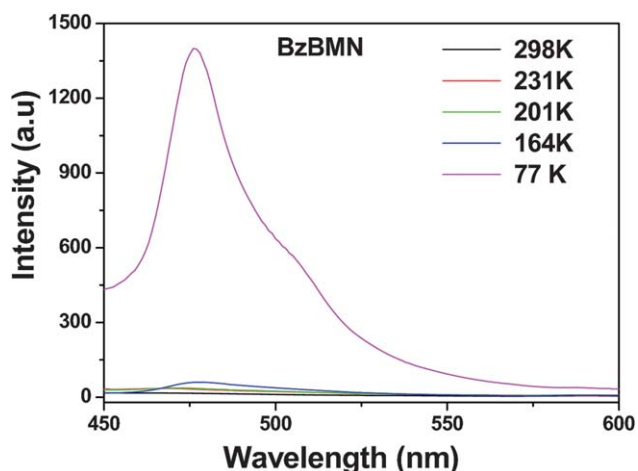


Fig. 3 PL spectra of BzBMN in ethanol/methanol solution (4/1, v/v) (50 μ M) at different temperatures.

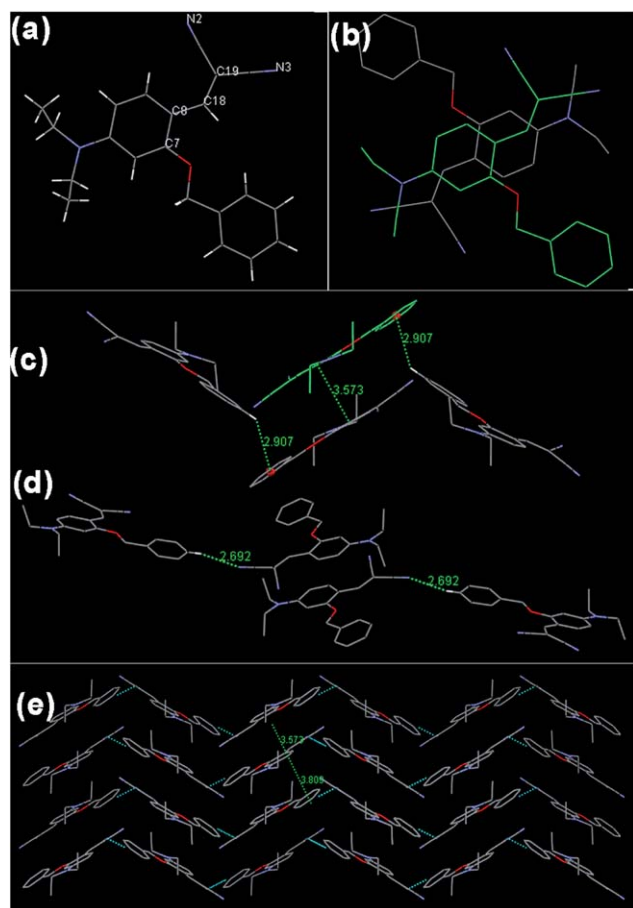


Fig. 4 Crystal structures of BzBMN: (a) single molecule structure. (b) Top view of the antiparallel dipole arrangement. (c) Side view of the antiparallel dipole arrangement and C–H \cdots π hydrogen bonds interactions. (d) C–H \cdots N hydrogen bonds interactions. (e) The crystal stacking images induced by hydrogen bond interactions. Hydrogen atoms have been omitted for clarity.

4.125 Å, 44.84° for BzFAN) are observed for both compounds. The more slipped stacking further weakens the π – π interaction and is in favour of the formation of a long-range ordered

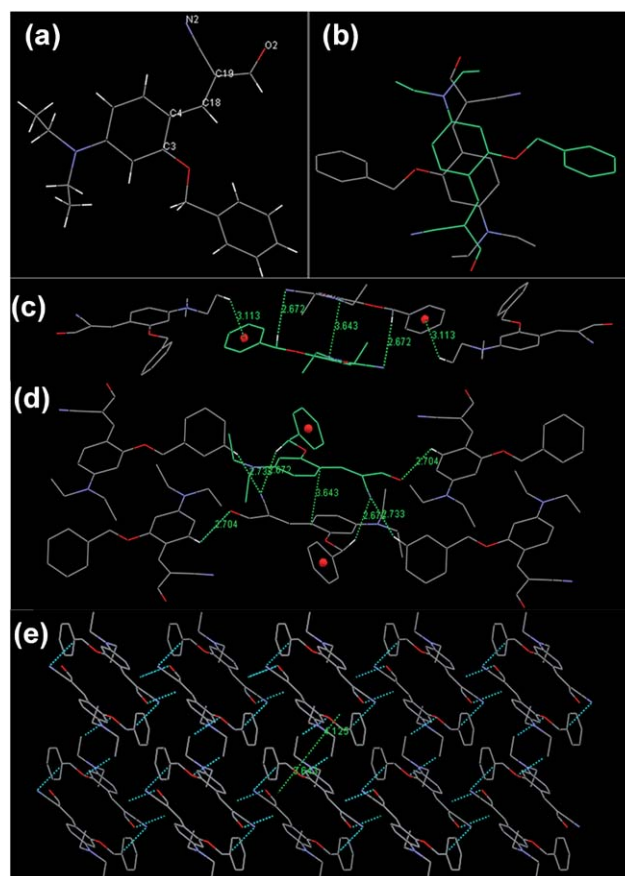


Fig. 5 Crystal structures of BzFAN: (a) single molecule structure. (b) Top view of antiparallel dipole arrangement. (c) Side view of antiparallel dipole arrangement and C–H \cdots π , C–H \cdots N hydrogen bonds interactions. (d) C–H \cdots O hydrogen bonds interactions. (e) The crystal stacking images induced by hydrogen bonds interactions. Hydrogen atoms have been omitted for clarity.

arrangement, such as *J*-aggregate,¹⁸ so we can consider that *J*-type aggregates are formed when larger aggregates are formed.

Time-resolved fluorescence measurements were performed to prove the existence of excitonic couplings. The fluorescence decay curves of BzBMN and BzFAN with different excitation

Table 2 Fluorescence lifetime of BzBMN and BzFAN in ethanol solution and crystal powder^a

Sample ^b	λ_{ex} (nm)	τ_1 (ns)	τ_2 (ns)	χ^2
B-sol	445	< 0.1		
B-cry	445	1.16 (0.04)	30.1 (0.96)	1.173
	500	1.37 (0.02)	33.1 (0.98)	1.125
F-sol	445	< 0.1		
F-cry	445	2.33 (0.47)	5.74 (0.53)	1.132
	500	4.60 (1.0)		1.043

^a Relative weights of lifetime are given in parentheses. The detection wavelength was 580 nm for BzBMN and 600 nm for BzFAN, respectively, except for in solution dispersed state that was 485 nm.

^b Abbreviations: B-sol = BzBMN in ethanol solution, B-cry = BzBMN crystal powder. F-sol = BzFAN in ethanol solution, F-cry = BzFAN crystal powder.

wavelengths are shown in Fig. S3† and the detailed data are listed in Table 2. In the good solution, the lifetime was obtained by monitoring at the monomer emission 485 nm. The decay of the monomer is too fast to be measured with our equipment (the limit is 0.1 ns). It should be less than 10 ps according to the result of *p*-*N,N*-dialkylaminobenzylidenemalononitriles, which have a similar main structure.¹³ In their crystalline forms, the two compounds show obviously longer lifetimes when monitoring at 580 and 600 nm. The long lifetime indicates the existence of new aggregation species or excitonic couplings. In addition, when excited at 445 nm or less, a double exponential fitting is more suitable for the decay curves of both compounds. When excited at 500 nm, a single lifetime model gives a better fitting for BzFAN. Although it is still a double exponential fitting for BzBMN, the contribution of the longer lifetime species obviously increases. The above results can be explained as follows: at a shorter excitation wavelength of 445 nm both high and low energy species or excitonic couplings are excited, however, at a longer excitation wavelength of 500 nm, only the low energy species or excitonic couplings with longer lifetime are active.

Fig. 4 and 5 also show that multiple hydrogen bonding interactions are involved in the crystals. For BzBMN, two kinds of interaction forces exist in the crystal (Fig. 4c–d). The phenyl ring of one molecular benzyl moiety interacts with the benzyl hydrogen of the neighboring column molecule through a C–H \cdots π hydrogen bond (2.907 Å). In addition, a C–H \cdots N hydrogen bond (2.692 Å) exists between the cyano moiety and the *para*-position benzyl hydrogen of the neighboring molecular layer. For BzFAN, there are three kinds of hydrogen bonding interactions in the crystal (Fig. 5c–d). A C–H \cdots π hydrogen bond (3.113 Å) formed between the terminal hydrogen of ethyl moiety and the phenyl core of the benzyl moiety connects the molecules of two adjacent columns together. Two C–H \cdots N (2.673 Å, 2.733 Å) and one C–H \cdots O (2.704 Å) hydrogen bonds exist between different molecular layers. These hydrogen bonding interactions restrict the rotations of the benzyl and malononitrile or nitrile acetaldehyde moiety, which enhances the emission efficiency of the BzBMN and BzFAN in aggregation state.

Thin solid films of BzBMN and BzFAN in PMMA were also prepared by spin-coating to further investigate the AIEE phenomenon. Fig. 6 shows the changes of the PL spectra with the

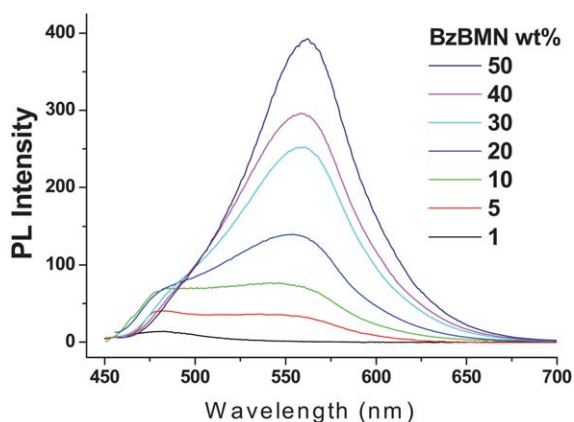


Fig. 6 PL spectra of BzBMN in a PMMA film with different doping concentrations (excited at 445 nm).

increasing concentrations of BzBMN in PMMA. It shows a weak emission peak at 483 nm, similar to that in ethanol, at very low doping concentrations (*e.g.* 1 wt %), which indicates that the molecules of BzBMN are monodispersed in the PMMA films. However, when the doping concentration is more than 5% wt, BzBMN exhibits dual fluorescence. The emission band can be resolved into two components, a short-wavelength emission band at \sim 483 nm from the monomer and a long-wavelength emission band at \sim 567 nm from the dimer (and other larger aggregates at higher concentrations).¹⁹ The long-wavelength emission intensity is also increased with increasing doping concentration. The emission wavelength is much shorter than that in the single crystal or nanoparticles. The reason for this phenomenon might be that the aggregates of BzBMN in the film are amorphous or lacking the long-range ordered arrangements, such as *J*-aggregation, as in the crystals.¹⁸ The emission of BzFAN in the PMMA film shows similar behavior (Fig. S4†). At a low doping concentration (1 wt %), its monomer emission appears at 485 nm, whereas with high doping concentration, the emission is intensified and red-shifted.

The crystal growth and self-assembling process

Time-dependent absorption and PL spectra were measured to reveal the crystal growth and self-assembly process of BzBMN and BzFAN in ethanol/water mixture (5/95) (Fig. 7). As shown in Fig. 7a, when the ethanol solution is injected into water, the absorption is peaked at 431 nm with a shoulder around 458 nm initially. With the time elapsing, the relative intensity of the shoulder peak gradually increases and it has become the main absorption band after 12 min. The blue shifted absorption band of 431 nm might mainly originate from the anti-parallel dimer structure. The new peak appearing at around 458 nm indicates the formation of aggregates larger than the dimer structure. Moreover, the maximum absorption wavelength gradually red shifts as time proceeds, suggesting the formation of long-range ordered arrangements with an extended π -electron conjugation system²⁰ (see discussion below). These results are also confirmed

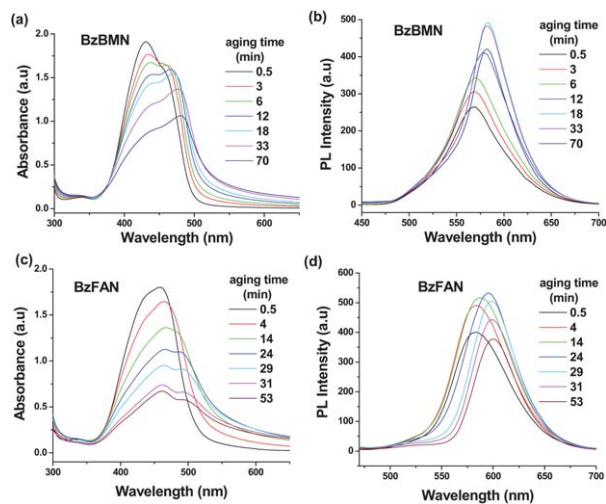


Fig. 7 Time-dependent absorption (a), (c) and PL (b), (d) spectra of BzBMN and BzFAN molecules (50 μ M) in ethanol/water (5/95) mixtures. Excited wavelength: 445 nm.

by the PL spectrum (Fig. 7b). Comparing to that of the monomer emission, the emission band of 567 nm is broad and structureless and shows a large red shift, which may originate from a dimer or small aggregates. Then the emission wavelength is further red-shifted as the crystals grow. The emission peak of 582 nm can be attributed to larger aggregates with an ordered crystal lattice structure. After 18 min, the emission peak wavelength remains unchanged but its intensity decreases due to the precipitation of nanoparticles. According to the spectral data, we consider that BzBMN might undergo a self-assembly process in ethanol/water mixtures with high water contents. When BzBMN molecules are injected into water, they would cluster together due to their hydrophobicity, producing some tiny crystal nuclei (small aggregates). With the growing of nuclei, larger aggregates such as *J*-aggregates are formed, which result in further red shift in its PL emission. BzFAN has a similar evolution trend as BzBMN in water/ethanol mixture with several differences in the details: (1) the blue-shifted absorption band at around 435 nm is not the maximum peak in the initial stage (Fig. 7c). This is attributed to a larger interplanar spacing (3.643 Å) between the BzFAN dimer than that of BzBMN (3.553 Å), weakening the π - π interaction between the dimer molecules; (2) the absorption wavelength of dissolved monomer at 461 nm remains essentially unchanged and the intensity is reduced more seriously due to the faster consumption of free BzFAN molecules in the mixed solvents;²⁰ (3) the intensity of a newly formed peak in the range of 483–503 nm is also reduced quickly as a result of faster precipitation (Fig. 7c). We can also find evidence in the reduced emission intensity in the red-shift range before it shifts to 600 nm (Fig. 7d) due to faster precipitation.

Scanning electron microscopic (SEM) studies were also carried out to study the crystal growth process (Fig. 8). Upon injection of the ethanol solution of BzBMN or BzFAN into water (5/95, v/v), small nanoparticles varying from 0.5 to 1 μm form immediately. Larger ordered crystal structures (microbelt for BzBMN and microtube for BzFAN) form 1 h later. Finally, almost perfect single crystal structures with smooth outer surfaces are observed 6 h later. The microbelts are 2–5 μm wide with length varying from *ca.* 15 to 40 μm . The microtubes are *ca.* 1.5–2 μm wide with length ranged from 10 to 50 μm . Such morphologic evolution corresponds well to the time-resolved spectra data.

As the tubular structure has many unique properties, the formation mechanism of the BzFAN nanotubes was further investigated. As mentioned, BzFAN molecules immediately aggregate into nanoparticles (Fig. 8b) when the ethanol solution is injected into water. The nanoparticles then grow into a sheet or belt-like structure (Fig. 9b–c), which is commonly observed in the organic nano/microtube formation process.²¹ These sheets or belts begin to curl up to give tubular structures (see black arrows in Fig. 9b–c) with the sheet broadening. A seaming process then occurs to give an open-ended rectangular hollow tube (Fig. 9d–h). Based on morphological features of the BzFANs nanostructures (Fig. 9b–h), such as the sharp ends and multilayer structures in Fig. 9d–e, we consider that the growth process of tubular crystals may also involve a self-assembly process, in which the initial sheets may serve as template and nucleation sites for the formation of secondary belt-like nanostructures perpendicular to the initial sheets. These eventually lead to the formation of the rectangular tubes. The edges along the tube axes (see

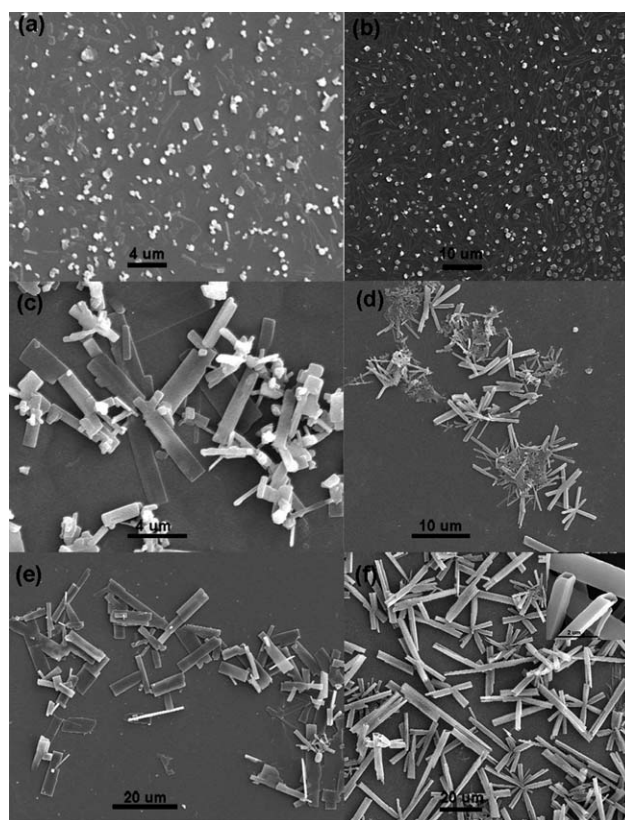


Fig. 8 SEM micrographs of BzBMN (a, c, e) and BzFAN (b, d, f) at several characteristic stages: (a) and (b) the immediately precipitated nanoparticles, (c) and (d) the nanostructures at around 1 h after injection, (e) and (f) almost completely grown structures at least 6 h after injection.

black arrows in Fig. 9h–i) of completed-growth tubes also indicate that a self-assembly process is involved in the growing process.

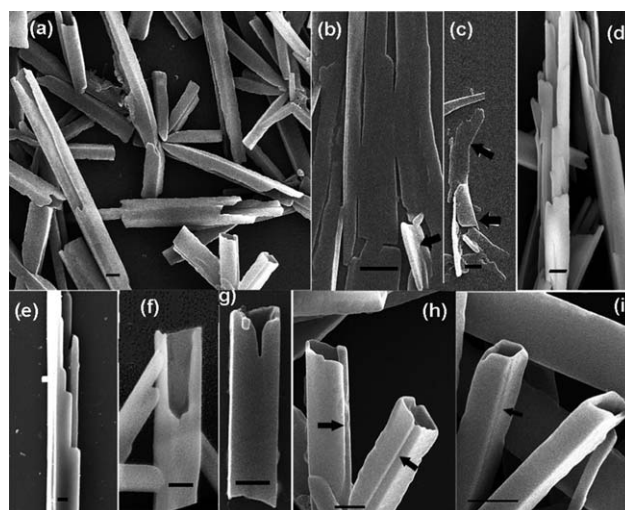


Fig. 9 SEM micrographs of BzFAN (a) microtubes containing different incomplete growth structure, (b) black arrows: belt structures, (c) black arrow: a sheet-like plane with one end has curled up, (d) and (e) the intermediate tubular structures composed by several sheets or belts, (f)–(h) defects in the open-ended and side feature, (i) microtubes of complete growth. Scale bars: 1 μm .

Conclusion

In summary, we have synthesized two compounds (BzBMN and BzFAN) with good yields and investigated their AIEE properties. Unlike typical AIEE active molecules, the two compounds have a simple molecular skeleton (2-benzyloxy-4-diethylaminobenzaldehyde) and few aromatic rings. It can be observed that the emission wavelength shows a great red shift and the intensity increases significantly in the solid state compared to that of their mono-disperse states. Crystal structure analysis revealed that dimers induced by dipole–dipole interaction and long-range ordered arrangements (*e.g.* *J*-aggregation) are responsible for the red shifted emissions in the crystals and nanosuspensions. Besides, intermolecular hydrogen bonding interactions, which restrict the intramolecular rotations and block the nonradiative processes, result in the enhanced emissions. It was also observed that BzBMN and BzFAN can easily assemble into single crystalline microbelts and microtubes respectively in ethanol/water mixtures.

Experimental

Materials and instruments

3, 3-diethoxypropionitrile, malononitrile, potassium *tert*-butoxide were purchased from Alfa Aesar Co. Other reagents were purchased from Beijing Chemical Regent Co. All of them were used directly without further purification. All solvents used for spectra measurement are of chromatographic grade. Ethanol was distilled from magnesium under dry nitrogen immediately prior to use for spectra measurement. ^1H NMR and ^{13}C NMR spectra were measured on a Bruker Avance II-400 spectrometer using CDCl_3 as the solvent and tetramethylsilane (TMS) as an internal reference. HR MS spectra were recorded on a Waters GCT Premier mass spectrometer. UV-vis spectra and fluorescence spectra were obtained with Hitachi U-3010 and F-4500 spectrophotometers, respectively. Time-resolved fluorescence lifetime experiments were performed by the time-correlated single-photon counting (TCSPC) system with Edinburgh Instruments FLS920 spectrophotometers. Fluorescence quantum yields (Φ_f) of BzBMN and BzFAN in solutions were estimated by using 9, 10-diphenylanthracene as the reference ($\Phi_f = 1.0$). The absolute fluorescence quantum yields of the crystals are measured with an integrating sphere. Field-emission scanning electron microscopy (FE-SEM) images were recorded on a Hitachi S-4300 instrument operated at an acceleration voltage of 10 kV.

Single crystals of the two compounds were prepared by slowly vaporizing their tetrahydrofuran (THF) solutions in a hexane atmosphere. The diffraction experiments were carried out on a Rigaku Saturn 724 diffractometer equipped with a Mo-K α source at about 170 K. Crystal structures were solved with direct methods and refined with a full-matrix least-squares technique, using the SHELXS software package. Mercury (CSD software) was used for crystal structure visualization.

Synthesis of 2-(benzyloxy)-4-(diethylamino)benzaldehyde (2)

Benzyl bromide (1.36 mL, 6.24 mmol) was added to a stirred mixture of **1** (1.0 g, 5.2 mmol) and K_2CO_3 (0.86 g, 6.24 mmol) in 30 mL of acetonitrile. After stirring at 70 °C for 4 h, the reaction

mixture was poured into water and extracted with ethyl acetate (4 × 30 mL). The combined organic extracts were washed with brine and dried (Mg_2SO_4). The crude product was purified by column chromatography (petroleum ether/ethyl acetate = 4 : 1) to give **2** (1.3 g, 88% yield). Mp: 70–71 °C; ^1H NMR (CDCl_3 , 400 MHz, ppm) δ : 1.154 (t, 6H, $J = 7.1$ Hz), 3.372 (q, 4H, $J = 7.1$ Hz), 5.174 (s, 2H), 6.071 (d, 1H, $J = 1.9$ Hz), 6.290 (dd, 1H, $J_1 = 8.9$ Hz, $J_2 = 1.9$ Hz), 7.325–7.458 (m, 5H), 7.734 (d, 1H, $J = 8.9$ Hz), 10.246 (s, 1H). HR MS (EI), m/z : 283.1576 (M^+ , Calcd for $\text{C}_{18}\text{H}_{21}\text{NO}_2$, 283.1572).

Synthesis of 2-(2-(benzyloxy)-4-(diethylamino)benzylidene) malononitrile (BzBMN)

To a 50 mL flask with two necks, **2** (0.5 g, 1.77 mmol) and ethanol (10 mL) were added. After **2** was dissolved, malononitrile (0.13 g, 1.95 mmol) and several drops of triethylamine were added. The mixtures were stirred at 60 °C for about 20 min to produce some orange-red precipitates. After cooling, the precipitates were filtrated. The crude products were recrystallized with ethanol and gave some orange-red crystal powders (0.53 g, 90% yield). Mp: 160–161 °C; ^1H NMR (CDCl_3 , 400 MHz, ppm) δ : 1.166 (t, 6H, $J = 7.1$ Hz), 3.401 (q, 4H, $J = 7.1$ Hz), 5.135 (s, 2H), 6.045 (d, 1H, $J = 1.9$ Hz), 6.336 (dd, 1H, $J_1 = 9.3$ Hz, $J_2 = 2.3$ Hz), 7.358–7.436 (m, 5H), 8.074 (s, 1H), 8.266 (d, 1H, $J = 9.3$ Hz); ^{13}C NMR (CDCl_3 , 100 MHz, ppm) δ : 160.9, 154.3, 150.9, 135.8, 130.7, 128.9, 128.5, 127.3, 117.2, 116.0, 109.7, 105.8, 94.2, 70.6, 68.6, 45.2, 12.6; HR MS (EI), m/z : 331.1688 (M^+ , calcd for $\text{C}_{21}\text{H}_{21}\text{N}_3\text{O}$, 331.1685).

Synthesis of (E)-3-(2-(benzyloxy)-4-(diethylamino)phenyl)-2-formyl-acrylonitrile (BzFAN)

Under a nitrogen atmosphere, **2** (1.0 g, 3.5 mmol) in 10 mL THF was added to a stirred mixture of potassium *tert*-butoxide (0.59 g, 5.3 mmol) and 3, 3-diethoxypropionitrile (0.60 g, 4.2 mmol) in 20 mL of THF. The mixture was stirred at 60 °C for 15 h. After the reaction was completed, 30 mL of water was added to the solution and the mixture was extracted with ethyl ether (3 × 30 mL). The organic phase was washed with brine and was evaporated under reduced pressure to gain reddish brown oils. Then, 20 mL of hydrochloric acid solution (1M) was added and the solution was refluxed for 1 h. After cooling, the reaction mixture was neutralized with alkali solution and was extracted with ethyl ether. The combined organic phase was washed with saturated brine, and dried with MgSO_4 . The concentrated mixture was purified by column chromatography (petroleum ether/ethyl acetate = 6/1). The crude product was recrystallized with ethanol-water and gave red crystalline solids (0.60 g, 51% yield). Mp: 168–169 °C. ^1H NMR (CDCl_3 , 400 MHz, ppm) δ : 1.169 (t, 6H, $J = 7.1$ Hz), 3.41 (q, 4H, $J = 7.1$ Hz), 5.185 (s, 2H), 6.102 (d, 1H, $J = 2.3$ Hz), 6.377 (dd, 1H, $J_1 = 9.3$ Hz, $J_2 = 2.3$ Hz), 7.260–7.422 (m, 5H), 8.283 (s, 1H), 8.447 (d, 1H, $J = 9.3$), 9.426 (s, 1H); ^{13}C NMR (CDCl_3 , 100 MHz, ppm) δ : 188.6, 161.5, 154.4, 151.4, 136.1, 131.9, 128.9, 128.4, 127.3, 117.1, 109.8, 105.9, 102.2, 94.4, 70.7, 45.2, 12.6; HR MS (EI), m/z : 334.1685 (M^+ , calcd for $\text{C}_{21}\text{H}_{22}\text{N}_2\text{O}_2$, 334.1681).

Acknowledgements

This work was supported by the National Natural Science Foundation of China (grant no. 21073213, 60778033), the Knowledge Innovation Program of the Chinese Academy of Sciences, the National High Technology Research and Development Program of China (863 Program) (grant no. 2008AA03A327), and the National Basic Research Development Program of China (973 Program) (grant no. 2009CB623703).

References

- (a) C.-T. Chen, Y. Wei, J.-S. Lin, M. V. R. K. Moturu, W.-S. Chao, Y.-T. Tao and C.-H. Chien, *J. Am. Chem. Soc.*, 2006, **128**, 10992; (b) R. Deans, J. Kim, M. R. Machacek and T. M. Swager, *J. Am. Chem. Soc.*, 2000, **122**, 8565; (c) T.-S. Yeh, T. J. Chow, S.-H. Tsai, C.-W. Chiu and C.-X. Zhao, *Chem. Mater.*, 2006, **18**, 832; (d) H.-C. Yeh, W.-C. Wu, Y.-S. Wen, D.-C. Dai, J.-K. Wang and C.-T. Chen, *J. Org. Chem.*, 2004, **69**, 6455.
- (a) S. W. Thomas, G. D. Joly and T. M. Swager, *Chem. Rev.*, 2007, **107**, 1339; (b) Z. J. Ning, Z. Chen, Q. Zhang, Y. L. Yan, S. X. Qian, Y. Cao and H. Tian, *Adv. Funct. Mater.*, 2007, **17**, 3799; (c) S.-J. Chung, K.-Y. Kwon, S.-W. Lee, J.-I. Jin, C. H. Lee, C. E. Lee and Y. Park, *Adv. Mater.*, 1998, **10**, 1112.
- (a) Z. Fei, N. Kocher, C. J. Mohrschladt, H. Ihmels and D. Stalke, *Angew. Chem. Int. Ed.*, 2003, **42**, 783; (b) C. L. Chiang, S. M. Tseng, C. T. Chen, C. P. Hsu and C. F. Shu, *Adv. Funct. Mater.*, 2008, **18**, 248; (c) S. F. Lim, R. H. Friend, I. D. Rees, J. Li, Y. Ma, K. Robinson, A. B. Holmes, E. Hennebicq, D. Beljonne and F. Cacialli, *Adv. Funct. Mater.*, 2005, **15**, 981; (d) C. Fan, S. Wang, J. W. Hong, G. C. Bazan, K. W. Plaxco and A. J. Heeger, *Proc. Natl. Acad. Sci.*, 2003, **100**, 6297; (e) B. S. Gaylord, S. Wang, A. J. Heeger and G. C. Bazan, *J. Am. Chem. Soc.*, 2001, **123**, 6417; (f) S. Hecht and J. M. J. Fréchet, *Angew. Chem. Int. Ed.*, 2001, **40**, 74.
- (a) J. Luo, Z. Xie, J. W. Y. Lam, L. Cheng, B. Z. Tang, H. Chen, C. Qiu, H. S. Kwok, X. Zhan, Y. Liu and D. Zhu, *Chem. Commun.*, 2001, 1740; (b) J. W. Chen, B. Xu, K. X. Yang, Y. Cao, H. H. Y. Sung, I. D. Williams and B. Z. Tang, *J. Phys. Chem. B*, 2005, **109**, 17086; (c) Z. Li, Y. Dong, B. Mi, Y. Tang, M. Häussler, H. Tong, Y. Dong, J. W. Y. Lam, Y. Ren, H. H. Y. Sung, K. S. Wong, P. Gao, I. D. Williams, H. S. Kwok and B. Z. Tang, *J. Phys. Chem. B*, 2005, **109**, 10061.
- (a) W. Z. Wang, T. T. Lin, M. Wang, T. X. Liu, L. L. Ren, D. Chen and S. Huang, *J. Phys. Chem. B*, 2010, **114**, 5983; (b) Z. J. Zhao, S. M. Chen, J. W. Y. Lam, P. Lu, Y. C. Zhong, K. S. Wong, H. S. Kwok and B. Z. Tang, *Chem. Commun.*, 2010, **46**, 2221; (c) Z. J. Zhao, S. M. Chen, X. Y. Shen, F. Mahtab, Y. Yu, P. Lu, J. W. Y. Lam, H. S. Kwok and B. Z. Tang, *Chem. Commun.*, 2010, **46**, 686.
- (a) B.-K. An, S.-K. Kwon, S.-D. Jung and S. Y. Park, *J. Am. Chem. Soc.*, 2002, **124**, 14410; (b) J. W. Chung, B. K. An and S. Y. Park, *Chem. Mater.*, 2008, **20**, 6750; (c) B.-K. An, S. H. Gihm, J. W. Chung, C. R. Park, S.-K. Kwon and S. Y. Park, *J. Am. Chem. Soc.*, 2009, **131**, 3950; (d) J. W. Chung, Y. You, H. S. Huh, B. K. An, S. J. Yoon, S. H. Kim, S. W. Lee and S. Y. Park, *J. Am. Chem. Soc.*, 2009, **131**, 8163; (e) S.-J. Yoon, J. W. Chung, J. Gierschner, K. S. Kim, M.-G. Choi, D. Kim and S. Y. Park, *J. Am. Chem. Soc.*, 2010, **132**, 13675.
- (a) H. Tong, Y. N. Hong, Y. Q. Dong, M. Haeussler, Z. Li, J. W. Y. Lam, Y. P. Dong, H. H. Y. Sung, I. D. Williams and B. Z. Tang, *J. Phys. Chem. B*, 2007, **111**, 11817; (b) M. Wang, G. Zhang, D. Zhang, D. Zhu and B. Z. Tang, *J. Mater. Chem.*, 2010, **20**, 1858; (c) Z. Li, Y. Q. Dong, J. W. Y. Lam, J. Sun, A. Qin, M. Häußler, Y. P. Dong, H. H. Y. Sung, I. D. Williams, H. S. Kwok and B. Z. Tang, *Adv. Funct. Mater.*, 2009, **19**, 905.
- (a) Y. Hong, J. W. Y. Lam and B. Z. Tang, *Chem. Commun.*, 2009, 4332; (b) Q. Zeng, Z. Li, Y. Dong, C. a. Di, A. Qin, Y. Hong, L. Ji, Z. Zhu, C. K. W. Jim, G. Yu, Q. Li, Z. Li, Y. Liu, J. Qin and B. Z. Tang, *Chem. Commun.*, 2007, 70.
- (a) H. Tong, Y. Dong, M. Haussler, Y. Hong, J. W. Y. Lam, H. H. Y. Sung, I. D. Williams, H. S. Kwok and B. Z. Tang, *Chem. Phys. Lett.*, 2006, **428**, 326; (b) H. Tong, Y. N. Hong, Y. Q. Dong, Y. Ren, M. Haussler, J. W. Y. Lam, K. S. Wong and B. Z. Tang, *J. Phys. Chem. B*, 2007, **111**, 2000; (c) Y. Liu, X. T. Tao, F. Z. Wang, X. N. Dang, D. C. Zou, Y. Ren and M. H. Jiang, *J. Phys. Chem. C*, 2008, **112**, 3975; (d) S. S. Palayangoda, X. C. Cai, R. M. Adhikari and D. C. Neckers, *Org. Lett.*, 2008, **10**, 281; (e) Q. Zhao, L. Li, F. Li, M. Yu, Z. Liu, T. Yi and C. Huang, *Chem. Commun.*, 2008, 685; (f) R. Hu, E. Lager, A. I. Aguilar-Aguilar, J. Liu, J. W. Y. Lam, H. H. Y. Sung, I. D. Williams, Y. Zhong, K. S. Wong, E. Peña-Cabrera and B. Z. Tang, *J. Phys. Chem. C*, 2009, **113**, 15845; (g) J. Xu, L. Wen, W. Zhou, J. Lv, Y. Guo, M. Zhu, H. Liu, Y. Li and L. Jiang, *J. Phys. Chem. C*, 2009, **113**, 5924; (h) C. K. Lim, S. Kim, I. C. Kwon, C. H. Ahn and S. Y. Park, *Chem. Mater.*, 2009, **21**, 5819; (i) W. X. Tang, Y. Xiang and A. J. Tong, *J. Org. Chem.*, 2009, **74**, 2163; (j) Y. Xu, P. Xue, D. Xu, X. Zhang, X. Liu, H. Zhou, J. Jia, X. Yang, F. Wang and R. Lu, *Org. Biomol. Chem.*, 2010, **8**, 4289.
- (a) Z. Wang, *Adv. Mater.*, 2003, **15**, 432; (b) R. Könenkamp, R. C. Word and M. Godinez, *Nano Lett.*, 2005, **5**, 2005; (c) J. Goldberger, A. I. Hochbaum, R. Fan and P. Yang, *Nano Lett.*, 2006, **6**, 973; (d) M. Law, L. E. Greene, J. C. Johnson, R. Saykally and P. Yang, *Nat. Mater.*, 2005, **4**, 455.
- (a) A. Datar, K. Balakrishnan, X. Yang, X. Zuo, J. Huang, R. Oitker, M. Yen, J. Zhao, D. M. Tiede and L. Zang, *J. Phys. Chem. B*, 2006, **110**, 12327; (b) J. Yu, F.-R. F. Fan, S. Pan, V. M. Lynch, K. M. Omer and A. J. Bard, *J. Am. Chem. Soc.*, 2008, **130**, 7196.
- K. Rurack, J. L. Bricks, G. Reck, R. Radeglia and U. Resch-Genger, *J. Phys. Chem. A*, 2000, **104**, 3087.
- (a) A. Safarzadeh-Amiri, *Can. J. Chem.*, 1984, **62**, 1895; (b) R. O. Loutfy and K. Y. Law, *J. Phys. Chem.*, 1980, **84**, 2803.
- H. Auweter, H. Haberkorn, W. Heckmann, D. Horn, E. Lüddecke, J. Rieger and H. Weiss, *Angew. Chem. Int. Ed.*, 1999, **38**, 2188.
- R. Rathore, S. V. Lindeman and J. K. Kochi, *J. Am. Chem. Soc.*, 1997, **119**, 9393.
- (a) T.-A. Chen, X. Wu and R. D. Rieke, *J. Am. Chem. Soc.*, 1995, **117**, 233; (b) J. Seo, S. Kim, S. H. Gihm, C. R. Park and S. Y. Park, *J. Mater. Chem.*, 2007, **17**, 5052.
- C. E. Smith, P. S. Smith, R. L. Thomas, E. G. Robins, J. C. Collings, C. Dai, A. J. Scott, S. Borwick, A. S. Batsanov, S. W. Watt, S. J. Clark, C. Viney, J. A. K. Howard, W. Clegg and T. B. Marder, *J. Mater. Chem.*, 2004, **14**, 413.
- N. S. S. Kumar, S. Varghese, C. H. Suresh, N. P. Rath and S. Das, *J. Phys. Chem. C*, 2009, **113**, 11927.
- K. Y. Law and R. O. Loutfy, *Macromol.*, 1981, **14**, 587.
- F. Wang, M.-Y. Han, K. Y. Mya, Y. Wang and Y.-H. Lai, *J. Am. Chem. Soc.*, 2005, **127**, 10350.
- (a) Y. S. Zhao, W. Yang, D. Xiao, X. Sheng, X. Yang, Z. Shuai, Y. Luo and J. Yao, *Chem. Mater.*, 2005, **17**, 6430; (b) H. Tang, J. P. Gao, Y. Xiong and Z. Y. Wang, *Cryst. Growth Des.*, 2006, **6**, 1559; (c) N. Chandrasekhar and R. Chandrasekar, *Chem. Commun.*, 2010, **46**, 2915.